Journal of Physics G:
Nuclear and Particle
Physics

PURPOSE-LED
PUBLISHING™

PAPER • **OPEN ACCESS**

Kaonic copper and fluorine absolute yields measurement with a CZT-based detection system at DAΦNE

To cite this article: Francesco Artibani *et al* 2026 *J. Phys. G: Nucl. Part. Phys.* **53** 095102

View the article online for updates and enhancements.

This content was downloaded from IP address 91.150.215.55 on 25/11/2026 at 12:43

Journal of Physics G: Nuclear and Particle Physics

Check for updates

OPEN ACCESS

RECEIVED
19 May 2026

REVISED
20 July 2026

ACCEPTED FOR PUBLICATION
27 August 2026

PUBLISHED
8 September 2026

Original content from this work may be used under the terms of the Creative Commons Attribution 4.0 licence.

Any further distribution of this work must maintain attribution to the author(s) and the title of the work, journal citation and DOI.

PAPER

Kaonic copper and fluorine absolute yields measurement with a CZT-based detection system at DAΦNE

Francesco Artibani[1,2,*], Simone Manti[1], Leonardo Abbene[3,1], Antonino Buttacavoli[3,1], Manuele Bettelli[4], Gaetano Gerardi[3], Fabio Principato[3,1], Andrea Zappettini[4], Massimiliano Bazzi[1], Giacomo Borghi[5,6], Damir Bosnar[7,1], Mario Bragadireanu[8], Marco Carminati[5,6], Alberto Clozza[1], Francesco Clozza[1,10], Raffaele Del Grande[11,1], Luca De Paolis[1], Carlo Fiorini[5,6], Ivica Friscic[7], Carlo Guaraldo[1,19], Mihail Iliescu[1], Masahiko Iwasaki[14], Aleksander Khreptak[12,13,1], Johann Marton[9], Pawel Moskal[12,13], Fabrizio Napolitano[15,16,1], Hiroaki Ohnishi[17], Kristian Piscicchia[18,1], Francesco Sgaramella[1], Michal Silarski[12], Diana Laura Sirghi[1,8,18], Florin Sirghi[1,8], Magdalena Skurzok[12,13,1], Antonio Spallone[1], Kairo Toho[17,1], Oton Vazquez Doce[1], Johann Zmeskal[19], Catalina Curceanu[1] and Alessandro Scordo[1]

[1] Laboratori Nazionali di Frascati, INFN, Via E. Fermi 54, 00044 Frascati, Italy
[2] Dipartimento di Matematica e Fisica, Università di Roma Tre, Via della Vasca Navale 84, 00146 Roma, Italy
[3] Dipartimento di Fisica e Chimica—Emilio Segrè, Università di Palermo, Viale Delle Scienze Edificio 18, 90128 Palermo, Italy
[4] Istituto Materiali per l'Elettronica e il Magnetismo, Consiglio Nazionale delle Ricerche, Parco Area delle Scienze 37/A, 43124 Parma, Italy
[5] Dipartimento di Elettronica, Informazione e Bioingegneria, Politecnico di Milano, Piazza Leonardo da Vinci 32, 20133 Milano, Italy
[6] INFN Sezione di Milano, Via Giovanni Celoria 16, 20133 Milano, Italy
[7] Department of Physics, Faculty of Science, University of Zagreb, Bijenička cesta 32, 10000 Zagreb, Croatia
[8] Horia Hulubei National Institute of Physics and Nuclear Engineering (IFIN-HH), No. 30, Reactorului Street, 077125 Magurele, Ilfov, Romania
[9] Atominstitut, Technical University Vienna, Stadionallee 2, 1020 Vienna, Austria
[10] Dipartimento di Scienze Matematiche Fisiche e Naturali, Università degli Studi di Roma Tor Vergata, Via Cracovia 90, 00133 Roma, Italy
[11] Faculty of Nuclear Sciences and Physical Engineering, Czech Technical University in Prague, Břehová 7, 115 19 Prague, Czech Republic
[12] Faculty of Physics, Astronomy, and Applied Computer Science, Jagiellonian University, Lojasiewicza 11, 30-348 Krakow, Poland
[13] Centre for Theranostics, Jagiellonian University, Kopernika 40, 31-501 Krakow, Poland
[14] RIKEN, 2–1 Hirosawa, Wako, Saitama 351-0198, Japan
[15] Dipartimento di Fisica e Geologia, Università degli studi di Perugia, Via A. Pascoli 06123 Perugia (PG), Italy
[16] INFN Sezione di Perugia, Via A. Pascoli – 06123 Perugia – Italia
[17] Research Center for Accelerator and Radioisotope Science (RARIS), Tohoku University, 1-2-1 Mikamine, Taihaku-ku 982-0826 Sendai, Japan
[18] Centro Ricerche Enrico Fermi—Museo Storico della Fisica e Centro Studi e Ricerche 'Enrico Fermi', Via Panisperna 89A, 00184 Roma, Italy
[19] Deceased.
[*] Author to whom any correspondence should be addressed.

E-mail: francesco.artibani@infn.it and francesco.artibani@uniroma3.it

Keywords: kaonic atoms, x-ray spectroscopy, CZT detector

Abstract

In this work, new measurements of absolute x-ray yields for several transitions in kaonic copper and, for the first time, in kaonic fluorine are reported. The data were collected by the SIDDHARTA-2 collaboration at the DAΦNE collider using a novel room-temperature cadmium zinc telluride (CZT) detection system. Detection efficiencies were evaluated through a dedicated Geant4 Monte Carlo simulation of the full experimental setup, enabling the extraction of absolute yields per stopped kaon. The measured yields exhibit a systematic dependence on the principal quantum number, reflecting the interplay between radiative transitions, Auger de-excitation, and strong-interaction-induced nuclear capture. In kaonic fluorine, a suppression of the $4\rightarrow3$ transition yield relative to higher-n transitions is observed, providing evidence for the onset of strong-interaction effects already at the $n = 4$ level. From this behaviour, a conservative lower limit on the corresponding strong-interaction width is derived. These results provide new quantitative constraints for cascade models of exotic atoms and extend experimental access to intermediate atomic

© 2026 The Author(s). Published by IOP Publishing Ltd

levels where strong-interaction effects are not directly observable via level shifts and widths. They also establish CZT-based detection as a powerful and versatile approach for high-resolution x-ray spectroscopy of kaonic atoms in collider environments.

1. Introduction

Kaonic atoms provide a relevant experimental framework to investigate strong interactions involving strangeness at low energies [1–5]. These exotic systems are formed when a negatively charged kaon stops inside a material and binds to a nucleus via the electromagnetic interaction. The capture occurs in a highly excited state, when the wavefunction overlap of the kaon with the outermost electron orbit of the target atom becomes significant [6].

The kaon subsequently undergoes an atomic cascade de-excitation, governed by the competition between three competing processes: Auger electron emission, which dominates at high principal quantum numbers where the kaon wavefunction is far from the nucleus; radiative x-ray emission, which becomes increasingly important at lower quantum numbers as the kaon approaches the nucleus; strong interaction induced nuclear capture, which becomes competitive only in the very last atomic levels when the kaon is sufficiently close to the nucleons to enable strong interaction between the meson and the hadrons. The relative importance of these three processes encodes information about both atomic and molecular dynamics [7] and the low-energy kaon–nucleon (K–N) and kaon-multinucleon (K-multiN) interaction [8].

Kaonic atom spectroscopy offers three complementary observables to constrain theoretical models of the strong interaction with strangeness [1, 4, 9]. The first two observables consist of the energy shifts (ϵ) and widths (Γ) of the last observable x-ray transitions, which provide direct information on the strong interaction in the final atomic levels. The third observable is the measurement of radiative yields of two consecutive transition, which, in some case, can provide access to the intrinsic widths Γ_u of levels where the strong interaction is too weak to be directly resolved by conventional x-ray detectors [10]. Both quantities serve as unique observables for testing theoretical models of K–N and K-multiN interactions in the nuclear medium [8, 11].

Moreover, measuring x-ray yields for transitions where the strong interaction is negligible, is essential for benchmarking cascade models. These models [7, 12, 13] aim to predict the de-excitation path of kaon through the atomic levels. To do so, they must account for complex and poorly understood processes, such as electron refilling, collisional effects, and the initial population distribution of atomic states. As a result, cascade models still suffer from significant uncertainties and rely on parameters previously constrained by direct yield measurements in exotic atoms [7].

Over the last decades, a new generation of kaonic atoms experiments performed at facilities such as DAΦNE, KEK, and J-PARC has significantly improved the spectroscopic information in the light kaonic atom mass region [14–18], enabling high-precision measurements of x-ray transitions. The intermediate and high mass region, however, still remains poorly explored, particularly regarding absolute yield measurements.

In this paper, the first measurements ever of absolute x-ray yields for kaonic fluorine ($Z = 9$) transitions in Teflon, and new measurements of kaonic copper transitions ($Z = 29$), performed by the SIDDHARTA-2 collaboration, are presented. These measurements span two different regions of the nuclear chart in terms of mass and density, and provide crucial test cases for cascade models. Furthermore, the kaonic fluorine measurements explore a regime where the strong interaction induced nuclear capture signature is observable at the measured atomic transitions. To achieve this goal, for the first time, a novel room-temperature cadmium zinc telluride (CZT) detection system [19–21], specifically developed by the collaboration for high-resolution kaonic atom x-ray spectroscopy, was deployed in a collider environment. The CZT detectors exhibited an energy resolution of 4% at 121 keV (FWHM), an energy linearity response better than 0.1%, and a detection efficiency higher than 90% in the 20–300 keV energy range [21] , relevant for this work, over several weeks of data taking in the DAΦNE collider.

Section 2 describes the experimental apparatus. Section 3 presents the data taking, analysis, and Monte Carlo simulations. Section 4 discusses the results, followed by the conclusions, section 5.

Table 1. Target materials together with their densities and thicknesses.

Material	Chemical composition	Density ($g\,cm^{-3}$)	Thickness (mm)
Teflon	C_2F_4	2.2	4
Copper	Cu	8.96	1

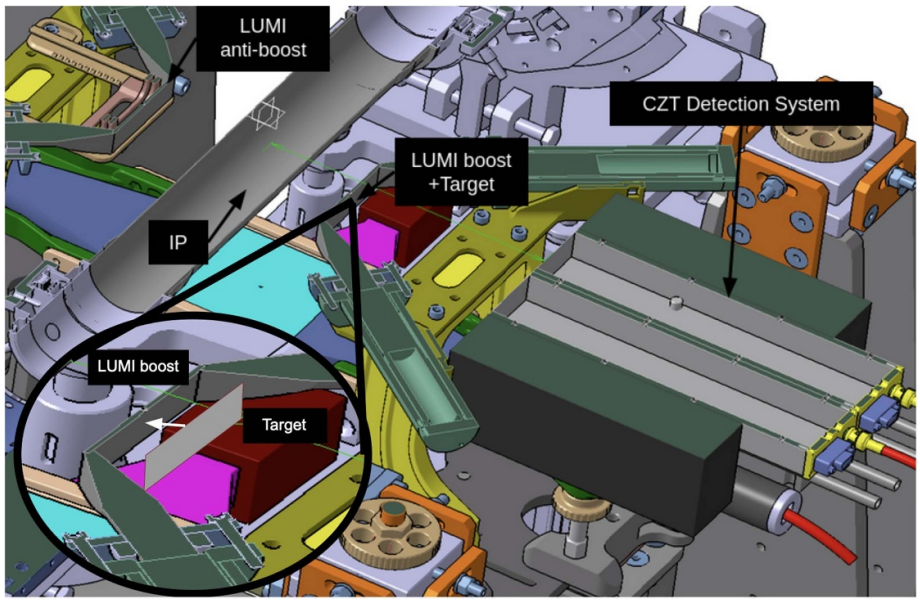

Figure 1. Schematic view of the experimental CZT detection system setup in DAΦNE used for the data taking presented in this work. Reproduced from [28].

2. CZT detectors in the SIDDHARTA-2 experiment at DAΦNE

The SIDDHARTA-2 experiment [4, 5, 9] is a dedicated apparatus for precision x-ray spectroscopy of kaonic atoms, installed at the interaction point (IP) of the DAΦNE electron–positron collider [22–25] at the Laboratori Nazionali di Frascati of the Istituto Nazionale di Fisica Nucleare (INFN-LNF).

DAΦNE operates as a ϕ-factory, with the centre-of-mass energy tuned to 1.022 GeV, corresponding to the mass of the ϕ meson. The ϕ meson decays almost at rest into pairs of charged kaons with a branching ratio of 48.9%. This feature provides a clean and nearly monochromatic source of low-momentum K^- mesons, well suited for the formation of kaonic atoms.

The SIDDHARTA-2 apparatus is described in detail in [26]. In the present work, only the subsystem relevant to the CZT-based detection of kaonic atom x-rays is discussed, corresponding to the configuration used in this work.

In the data-taking campaigns, the CZT detection system [19–21] was installed in the plane of the collider rings, in their inner part. The system consists of eight quasi-hemispherical CZT detectors with dimensions of $13 \times 15 \times 5$ mm^3, grown using the travelling heater method by REDLEN Technology (Canada). The detectors are housed in a thin aluminium enclosure equipped with a 0.27 mm-thick aluminium window, which contains both the detector crystals and the front-end electronics. The enclosure was positioned at a distance of 29.3 cm from the collider IP.

Between the beam pipe and the CZT detection system, a $80 \times 40 \times 2$ mm^3 Scionix BC-408 organic scintillator coupled to two photomultiplier tubes via plastic light guides was installed [27]. This detector (LUMI boost), in combination with an identical module placed on the opposite side (LUMI antiboost), was used for luminosity monitoring and for charged kaon selection via time-of-flight techniques as discussed in section 3. The scintillator was located at a distance of 10.2 cm from the IP.

The targets, in which the negative kaons are stopped to form kaonic atoms, consisted of two different material foils, and were placed downstream of the plastic scintillator, facing the detector enclosure. Table 1 summarizes the thickness and the main characteristics of each target.

In figure 1 the experimental setup during all the runs is shown.

Table 2. Summary of the runs used in the data analysis for each target.

Target	Delivered integrated luminosity (pb^{-1})	Active detectors (for data analysis)
Cu	35 ± 1.8	8
	66 ± 3.4	7
Teflon	33 ± 1.7	6
	41 ± 2.1	6

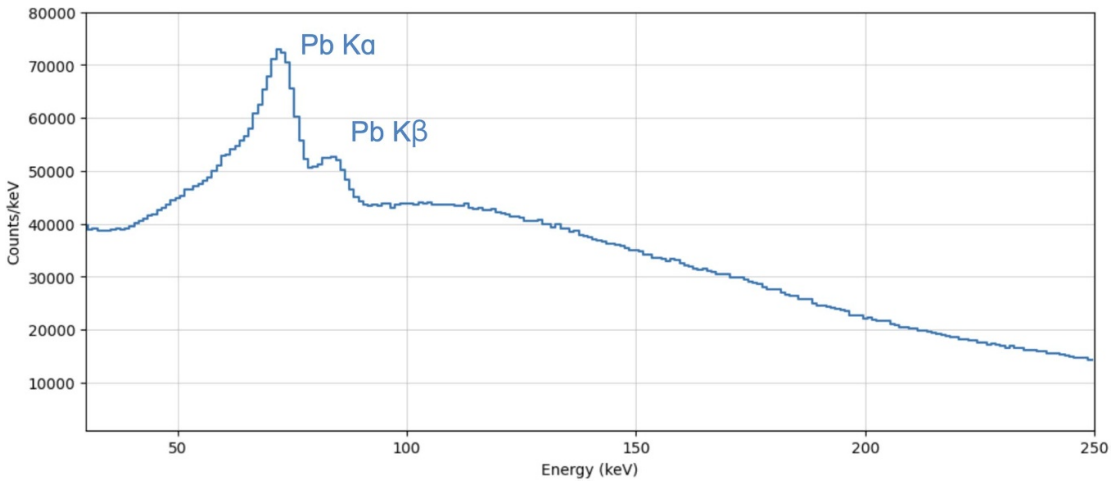

Figure 2. Energy spectrum of triggered events collected during the second run with copper target.

3. Data taking and analysis

Being used for the first time in a collider, the CZT detection system underwent an initial commissioning, testing, and optimization phase in which the stability of the operations [21] and the timing performances [28] were accurately tested. As a result the number of CZT detectors actively operating and used for physics analysis varied across the data-taking.

Table 2 summarizes the 2024 data-taking periods considered in the present analysis, together with the corresponding delivered integrated luminosity and systematic errors, extrapolated following [27], and the number of CZT detectors included in the data analysis for each target.

3.1. Data selection

Events are selected by requiring a trigger coincidence between the two luminometers and the CZT detector. For each triggered event, the full waveform is recorded over a 10 μs snapshot window. The data acquisition system ensures 99% throughput up to 1500 cps, which corresponds to the maximum input counting rate measured during beam-on conditions [21]. Detector saturation, which could arise from very rare high-energy events ($<$0.001% in the final triggered dataset) or from pile-up, was effectively mitigated by the charge-sensitive preamplifier's resistive feedback, characterized by an exponential decay constant of 100 μs, which restores the baseline after large energy depositions, and by the trigger logic, which suppresses uncorrelated background and keeps the effective counting rate well within the operational range of the system. Under these operating conditions, saturation and pile-up were found to be negligible and did not affect the quality of the energy spectra [21, 28]. A typical raw energy spectrum corresponding to one of the data-taking periods is shown in figure 2.

Lead fluorescence lines (75 keV and 85 keV) are observed over the background. To extract x-rays originating from kaonic atom transitions, a dedicated data-selection procedure, based on timing information from both the luminometers and the CZT detectors, was applied as described in [28].

Since the primary goal of this work is the measurement of absolute yields, conservative and uniform selection criteria were applied to all datasets, in order to maximise efficiency over purity. The kaon time selection window was chosen to be 1 ns wide, while a time window of 170 ns width was applied to the CZT-luminometer time difference distribution for all targets and data-taking periods (see [28] for technical details).

3.2. Fit functions

The final energy spectra, calibrated following the procedure described in [21], were summed target-by-target and subsequently analysed to extract the energy and the number of events for each kaonic atoms x-ray transitions.

The background contribution was modelled using the function

$$f_{bkg}(x) = a + bx + c\exp(dx) + \mathrm{erfc}\left(\frac{e-x}{f}\right), \tag{1}$$

where the linear part (a and b parameters) describes the electronics baseline, the exponential part (c and d parameters) describes background generated by photons and electrons undergoing Compton scattering, and the complementary error function part (e and f parameters) accounts for the low-energy cutoff resulting from the presence of shielding and electronic components. This background was previously validated in [21] using beam-on data with a known radioactive source.

The x-ray peaks corresponding to kaonic atom transitions were described by Gaussian functions,

$$f_{\mathrm{peak}}(x) = N\exp\left(-\frac{(x-\mu)^2}{2\sigma^2}\right), \tag{2}$$

where N is the peak area, μ the centroid energy, and σ the detector resolution.

For the 75 keV peak arising from fluorescence of the lead shielding after activation, an additional low energy tail component accounting for incomplete charge collection in the CZT detectors was included. The tail was modelled as

$$f_{\mathrm{tail}}(x) = \epsilon N\exp\left(\frac{x-\mu}{\beta\sigma}\right) erfc\left(\frac{x-\mu}{\sqrt{2}\sigma} + \frac{1}{\sqrt{2}\beta}\right), \tag{3}$$

where ϵ represents the relative intensity of the tail and β its characteristic width.

For all other fitted peaks, the tail contribution was found to be statistically insignificant and was therefore omitted.

To account for the intrinsic resolution of the detector, the σ parameters of the Gaussian, were described as a function of the energy, following the formula

$$\sigma(x) = \sqrt{a_\sigma \cdot x + b_\sigma} \tag{4}$$

with a_σ and b_σ free parameters common to all the peaks.

3.3. Fit method

The two spectra corresponding to copper and Teflon target were simultaneously fitted, by means of χ^2 minimisation, with the following common parameters:

- The Gaussian σ parameters a_σ and b_σ;
- The mean of the lead Kα and Kβ fluorescence peaks;
- The relative amplitude of the lead Kβ with respect to the Kα fluorescence peak;
- The tail parameters ϵ and β for the lead Kα fluorescence peak;

while the background and kaonic atom transition parameters were kept independent for each dataset. The fit was performed in this way to have a better description of the background due to the lead fluorescence (Pb Kα and Pb Kβ fluorescence lines), and of the parameters of the energy resolution.

3.4. Results

The results of the fit are presented in figures 3 and 4. The reduced chi-squared of the simultaneous fit resulted to be $\chi^2_{\mathrm{red}} = 1.27$.

The measured energies and the corresponding numbers of events for the observed kaonic atom transitions, as obtained from the fits, are summarized in table 3.

The systematic uncertainties were evaluated by repeating the fitting procedure under different analysis conditions, following the approach already adopted in [28], additional details were added in supplementary data.

Table 3. Energy and number of events extracted from the fits, with the corresponding theoretical energies calculated using the MCDFGME code [29].

Transition	Measured energy ± stat. ± sys. (keV)	Theoretical energy (keV)	Number of events ± stat. ± sys.
		Fluorine	
KF 5 → 4	23.34 ± 0.34 ± 0.11	23.33	488 ± 72 ± 30
KF 4 → 3	50.14 ± 0.54 ± 0.15	50.59	427 ± 74 ± 42
		Copper	
KCu 8 → 7	52.89 ± 0.50 ± 0.30	52.63	578 ± 84 ± 38
KCu 7 → 6	80.89 ± 0.98 ± 0.60	81.17	1078 ± 297 ± 190
KCu 6 → 5	134.48 ± 0.35 ± 0.31	134.81	1206 ± 132 ± 42

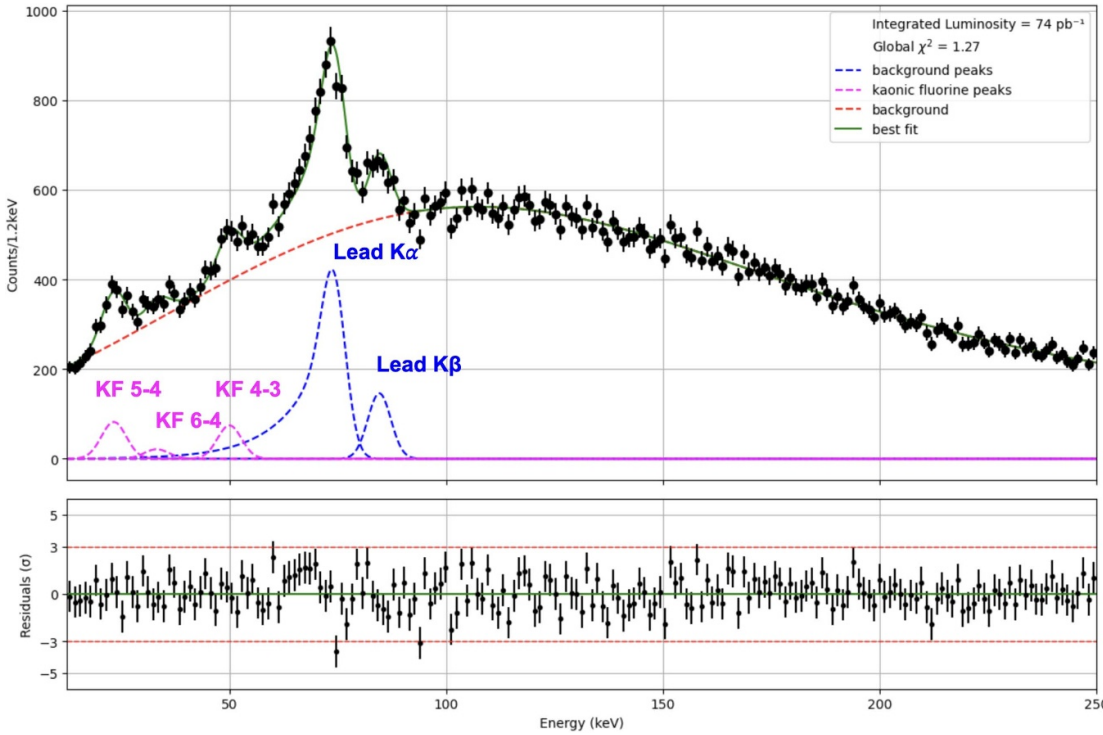

Figure 3. Upper: Kaonic fluorine energy spectrum and fit. The experimental counts are shown in black, with error bars representing the statistical uncertainty on the bin counts. The contributions from lead fluorescence transitions are shown in blue, kaonic atom transitions in magenta, the background in dashed red, and the total fit in green. Lower: Relative residuals of the fit.

The statistical significance of the peaks reported in table 3 was evaluated using a χ^2-based hypothesis test, where the nominal fit was compared to a fit with the peak amplitude fixed to zero. The significance is given by $\sqrt{\Delta\chi^2}$, with $\Delta\chi^2 = \chi^2_{\text{no-signal}} - \chi^2_{\text{signal}}$. Only transitions with a significance above the 3σ threshold are included in the table. The KF 6 → 4 transition, visible in figure 3, was tested with the same procedure and yielded $\Delta\chi^2 = 2.2$, equivalent to a significance of 1.5σ, below the 3σ threshold. It is therefore not reported in table 3.

In the spectrum obtained with the Teflon target, no transitions from kaonic carbon were observed, even though the KC 4→3 and KC 3→2 transitions are expected around 20 keV and 65 keV, respectively. The absence of these lines can be attributed to two concurring effects. First, kaons are preferentially captured by fluorine over carbon, due to the higher atomic charge and abundance of fluorine in the Teflon molecule, a behaviour consistent with observations in [30]. A discussion of the different capture models is deferred to the next section. Second, strong interaction effects at the $n = 4$ and $n = 3$ levels of kaonic carbon are expected to broaden and suppress the x-ray yield of these transitions.

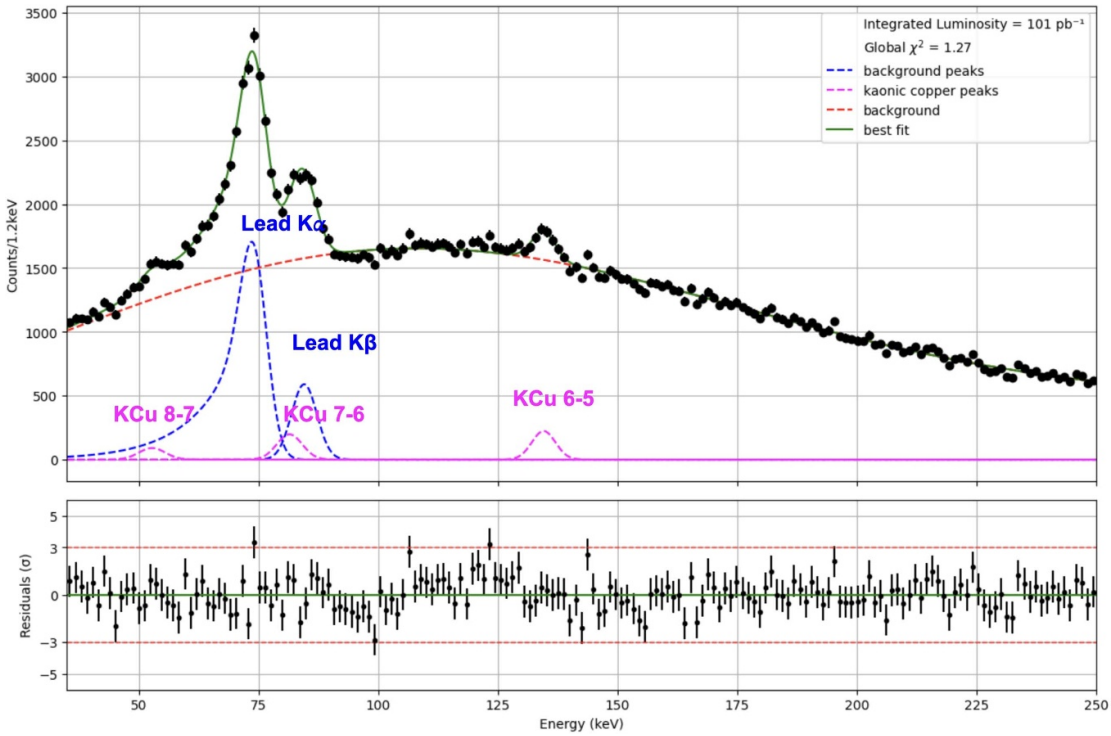

Figure 4. Upper: Kaonic copper energy spectrum and fit. The experimental counts are shown in black, with error bars representing the statistical uncertainty on the bin counts. The contributions from lead fluorescence transitions are shown in blue, kaonic atom transitions in magenta, the background in dashed red, and the total fit in green. Lower: Relative residuals of the fit.

3.5. Monte Carlo simulation

In order to account for the geometrical acceptance and the detector response, and to determine the number of kaons stopped in the target, essential ingredients for the extraction of absolute x-ray yields per stopped kaon, a Monte Carlo simulation based on the GEANT4 toolkit was developed. The simulation reproduces the experimental setup, including the exact geometry of the CZT crystals and their spacing, the aluminium entrance window, the luminometer system, and the DAΦNE beam pipe.

The simulation starts with the production of a ϕ meson at the IP. Its four-momentum is reconstructed from the sum of the electron and positron four-momenta, each smeared with a Gaussian energy spread of $\sigma = 0.2$ MeV around the nominal beam energy of 510 MeV. The crossing angle of 50 mrad between the beams, responsible for the meson's boost present in DAΦNE, is also taken into account. Since the beam energy spread is much narrower than the ϕ width, the generated invariant mass of the ϕ M_{inv} is sampled according to the probability $P(M_{\text{inv}}) = \text{BW}(M_{\text{inv}})/\text{BW}(m_\phi)$, where BW is a Breit-Wigner function with $M = m_\phi$ and $\Gamma = \Gamma_\phi$ taken from the PDG [31]. Once the ϕ mass is defined, the interaction vertex is smeared with Gaussian distributions of $\sigma_x = 2$ mm, $\sigma_y = 20$ μm, and $\sigma_z = 1$ cm, reflecting the beam spot size. The subsequent ϕ decays, including the decay into charged kaon pairs, are simulated, and the transport of the kaons through the experimental apparatus is tracked until their decay or stopping in the target or surrounding materials.

Whenever a negatively charged kaon stops in the target material, and forms a kaonic atom, the x-ray transitions of interest within the energy range of the CZT detectors are isotropically generated with a radiative yield set to 100% (i.e. used as a normalization reference for efficiency determination). This choice provides a normalization reference, allowing the experimental yields to be extracted by comparison with the simulated x-ray intensities.

Being teflon a compound element (C_2F_4), kaons stopped in the material can bind to either fluorine or carbon nuclei, and the exact capture process remains uncertain. In [32], kaons were assumed to stop on the elements of a compound in proportion to the atomic charge fraction, which for fluorine gives a factor $f_Z = Z_F \cdot N_F/(Z_F \cdot N_F + Z_C \cdot N_C) = 0.75$, with Z_F and Z_C atomic number of fluorine and carbon, and N_F and N_C atomic abundance in Teflon respectively for fluorine and carbon. This approach was originally suggested by Fermi and Teller in their study of exotic atoms, but significant deviations from this behaviour were found in muonic and pionic atoms [33]. The SIDDHARTA collaboration,

Table 4. Kaonic copper absolute yields per kaon stopped, with the corresponding statistical and systematic error.

Transition	Yield (%) ± stat. ± sys.
KCu $8 \rightarrow 7$	$17.6 \pm 2.6\ ^{+1.5}_{-1.5}$
KCu $7 \rightarrow 6$	$18.5 \pm 5.1\ ^{+3.0}_{-3.0}$
KCu $6 \rightarrow 5$ *	$21.4 \pm 2.3\ ^{+1.3}_{-3.0}$

* The KCu $6 \rightarrow 5$ transition in the measurement is contaminated by the KCu $8 \rightarrow 6$ transition. This contribution was considered in the systematics (see text).

Table 5. Kaonic fluorine absolute yields, with the corresponding statistical error and systematic error.

Transition	Yield in Teflon (%) ± stat. ± sys.	Yield in F with $f_Z = 0.75$ (%) ± stat. ± sys.	Yield in F with $f_N = 0.66$ (%) ± stat. ± sys.
KF $5 \rightarrow 4$	$9.8 \pm 1.5 \pm 0.6$	$13.1 \pm 2.0 \pm 0.9$	$14.8 \pm 2.3 \pm 1.1$
KF $4 \rightarrow 3$	$7.5 \pm 1.3 \pm 0.8$	$10.0 \pm 1.7 \pm 0.9$	$11.4 \pm 1.9 \pm 1.1$

in measurements on Kapton ($C_{22}H_{10}N_2O_5$) [15], used instead a factor proportional to the number of nuclei in the molecule, which for fluorine in Teflon gives $f_N = N_F/(N_F + N_C) = 0.66$. Given these theoretical uncertainties, it was decided to generate an x-ray every time a kaon stops in the compound, and to correct the result a posteriori using both factors.

3.6. Yields measurement

Following the approach adopted in previous kaonic atom experiments [34], the absolute x-ray yield Y per stopped kaon for a given transition is defined as the ratio between the experimental and simulated number of x-rays from kaonic atoms, normalized to the kaon pairs detected by the luminometers

$$Y_{\text{rad}} = \frac{N^{\text{EXP}}_{\text{X-ray}}/N^{\text{EXP}}_{\text{KLUMI}}}{N^{\text{MC}}_{\text{X-ray}}/N^{\text{MC}}_{\text{KLUMI}}}, \tag{5}$$

where $N^{\text{EXP}}_{\text{X-ray}}$ and $N^{\text{EXP}}_{\text{KLUMI}}$ denote, respectively, the number of x-ray events observed for the selected kaonic atom transition and the number of kaons measured by the luminometer in the experimental data. The quantities $N^{\text{MC}}_{\text{X-ray}}$ and $N^{\text{MC}}_{\text{KLUMI}}$ are the corresponding values obtained from the Monte Carlo simulation.

The systematic errors from the Monte Carlo simulation were evaluated by moving the target from its nominal position (just downstream of the LUMI) by 0.5 mm, varying the target thickness by ±0.1 mm, and including the statistical uncertainty on the simulated counts.

In table 4 the measured yields for kaonic copper are presented.

In kaonic copper, as in several other kaonic atoms [33], the energies of the $6 \rightarrow 5$ transitions overlap with those of the $8 \rightarrow 6$ transitions, making them experimentally indistinguishable for a yield measurement. Nevertheless, the $\Delta n = 2$ transitions are disfavoured by selection rules, and their contribution to the total yield is approximately 10% of that of the principal $\Delta n = 1$ transition [33]. In the present case, the latter is the $8 \rightarrow 7$ transition, measured to be 17.6%. Consequently, the contribution of the $8 \rightarrow 6$ transition to the overall yield of the $6 \rightarrow 5$ transition is expected to be of the order of 2%–3%, considered in the systematic error.

The measured yields for kaonic fluorine are presented in table 5.

The measured yield per kaon stopped in copper for the $8 \rightarrow 7$ and $6 \rightarrow 5$ in table 4 represent the new most precise measurement, and together with the $7 \rightarrow 6$ show a good compatibility with the old measurement done in [33], while the yield for the transitions in table 5 represent the first measurement ever.

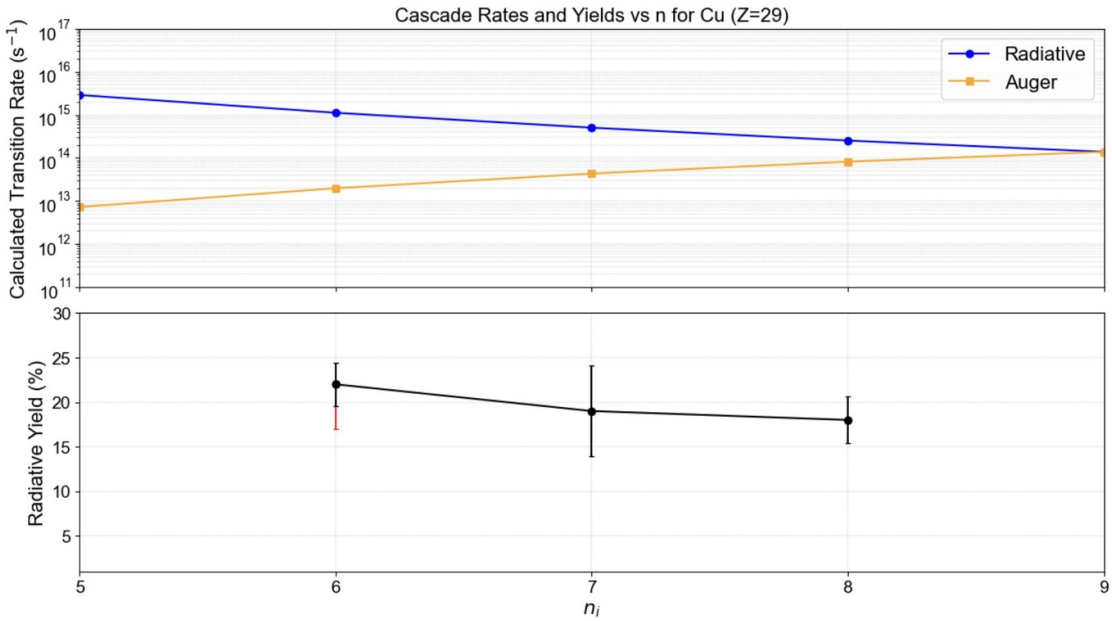

Figure 5. Upper panel: radiative (blue) and Auger K-shell (orange) transition rates for circular states ($l = n - 1$) with $\Delta n = 1$. Lower panel: measured x-ray yield per stopped kaon. A conservative systematic uncertainty of −5% (red) was assigned to the 6 → 5 transition yield due to the uncertainty in the 8 → 6 transition's yield (see text).

4. Discussion

The intensity of the spectral lines, and consequently the x-ray yields per stopped kaon, produced by kaonic atoms as a function of the principal quantum number result from a complex interplay between radiative transitions, Auger de-excitation from the electronic shells, and nuclear capture induced by the strong interaction.

From cascade considerations [13], the radiative transition rate increases as the principal quantum number n_i decreases, while the Auger rate shows the opposite trend, becoming more important at higher n_i. The nuclear capture probability associated with the strong interaction, on the other hand, remains negligible at large atomic radii and starts to increase only when the kaon wave function significantly overlaps with the nuclear density. Within this framework, the experimental x-ray yields encode the cumulative effect of these competing processes.

For kaonic copper, this trend is confirmed by the observations in table 5: the yields increase smoothly as n_i decreasing, consistent with a radiative-dominated cascade in which Auger processes lose importance, and nuclear capture contribution is negligible.

A different behaviour is observed for kaonic fluorine. The yield of the 4 → 3 transition is suppressed with respect to the higher-n transitions, suggesting the onset of strong interaction effects at the $n = 4$ level.

To support this interpretation, figures 5 and 6 show the calculated radiative and Auger rates for circular transitions with $\Delta n = 1$ from a given initial level n_i, alongside the measured x-ray yields, for kaonic copper and kaonic fluorine, respectively. The upper panels display the calculated rates, while the lower panels show the measured yields per stopped kaon.

Following [35], as done in [36], the radiative rates $\Gamma_{\rm rad}$ were derived using equation (6), assuming electric dipole transitions, hydrogenic wave functions with reduced mass μ:

$$\Gamma^{\rm rad}_{(n,l)\to(n',l\pm1)} = \frac{4\mu Z^4\alpha^3}{3}\cdot\left|\mathcal{R}^{(n,l)}_{(n',l\pm1)}\right|^2\cdot\left(\Delta E_{(n,n')}\right)^3, \tag{6}$$

where Z is the atomic number, μ the reduced mass of the exotic atom system, α the fine structure constant, and $\mathcal{R}^2$ is the dipole radial integral evaluated analytically.

The Auger K-shell rate was estimated assuming a single K-shell electron with effective nuclear charge $Z_e = Z - 1$ with the following formula:

$$\Gamma^{{\rm Aug},1s}_{(n,l)\to(n',l\pm1)} = \frac{16}{3}\cdot\frac{\pi Z_e^2}{\mu^2 Z^2}\cdot\frac{l}{2l+1}\cdot\left|\mathcal{R}^{(n,l)}_{(n',l\pm1)}\right|^2\cdot\frac{y_K^2}{1+y_K^2}\cdot\frac{\exp\left(y_K\left(4\tan^{-1}y_K-\pi\right)\right)}{\sinh\left(\pi y_K\right)}, \tag{7}$$

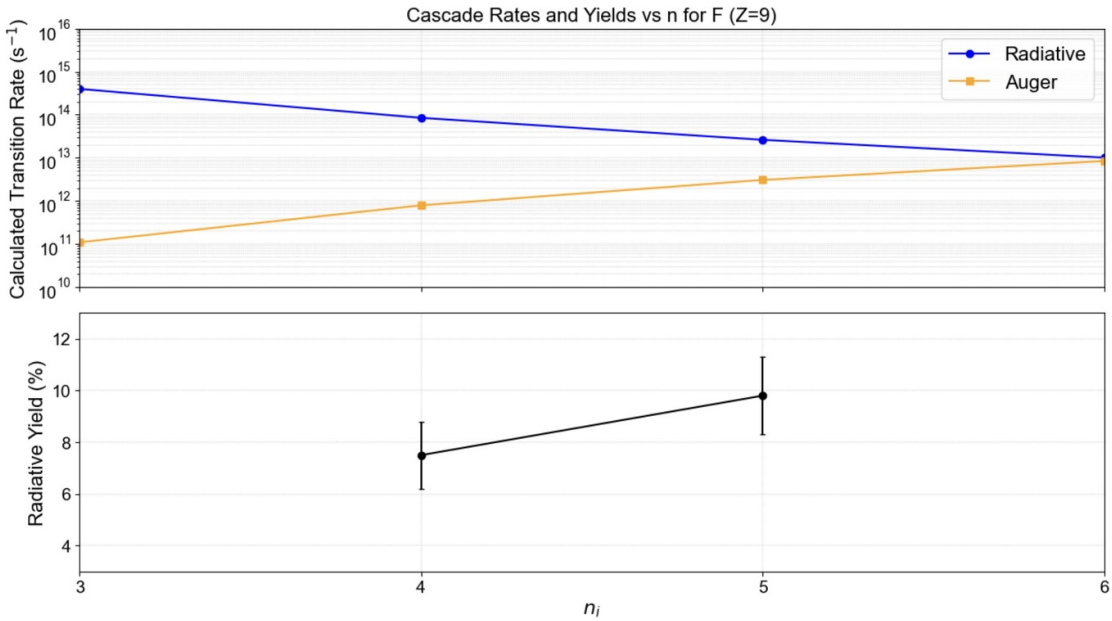

Figure 6. Upper panel: radiative (blue) and Auger K-shell (orange) transition rates for circular states ($l = n - 1$) with $\Delta n = 1$ starting from level n_i in kaonic fluorine. Lower panel: measured x-ray yield per stopped kaon.

where $\mathcal{R}^2$ is the dipole radial integral, and y_K is the Sommerfeld parameter:

$$y_K = \frac{Z_e}{\sqrt{2E_K}} \tag{8}$$

with E_K is the electron energy in the K shell.

Looking at figure 6, the observed suppression of the $4 \to 3$ yield in kaonic fluorine suggests that nuclear capture already contributes at $n = 4$. The strong interaction width Γ_{strong} for a level n can be estimated from the radiative yield attenuation, assuming negligible Auger rates [8]:

$$\Psi_n = \frac{\Gamma_{rad}^{(n)}}{\Gamma_{rad}^{(n)} + \Gamma_{strong}^{(n)}} = \frac{Y_{n\to n-1;rad}}{\sum_{N>n}(Y_{N\to n;rad} + (Y_{N\to n;Aug})}, \tag{9}$$

where the sum in the denominator runs over all transitions feeding level n from higher-lying states. A determination of Γ_{strong} would therefore require a full cascade calculation to evaluate this feeding contribution.

In the absence of a dedicated cascade model for kaonic fluorine, we instead use the measured x-ray yields per stopped kaon to set a constraint on Γ_{strong} for $n = 4$. From the experimental data we obtain the ratio

$$R = \frac{Y_{4\to 3;rad}}{Y_{5\to 4;rad}} = 0.77 \pm 0.17. \tag{10}$$

The relative yield of the $4 \to 3$ transition includes not only direct population from the $5 \to 4$ transition, but also additional feeding from higher levels (e.g. $6 \to 4$, $7 \to 4$, …), which are not accounted for in the denominator. As a consequence, the ratio R overestimates the true radiative yield of the $n = 4$ level,

$$\Psi_4 = \frac{\Gamma_{rad}^{(4)}}{\Gamma_{rad}^{(4)} + \Gamma_{strong}^{(4)}}, \tag{11}$$

implying $R \geqslant \Psi_4$. This leads to the inequality

$$\Gamma_{strong}^{(4)} \geqslant \Gamma_{rad}^{(4)} \left(\frac{1}{R} - 1\right). \tag{12}$$

To obtain a conservative lower limit, we consider the maximum value of R within one standard deviation, $R_{\max} = 0.94$, yielding

$$\Gamma^{(4)}_{\text{strong}} > 0.056 \cdot \left(\frac{1}{0.94} - 1 \right) = 0.0036 \text{ eV} \quad (90\% \text{ C.L.}), \tag{13}$$

with $\Gamma^{(4)}_{\text{rad}} = 0.056$ eV, calculated using equation (6).

This result provides the first indication of strong interaction effects in this system. A precise quantification of the strong-interaction width at the $n = 4$ level requires a reliable cascade model, on which the collaboration is currently working; nevertheless, some preliminary considerations can already be made. The Auger rates in equation (10) are negligible, being about one order of magnitude lower than the radiative rates (see figure 6). Similarly, transitions with $\Delta n > 2$ can be safely neglected. The $6 \rightarrow 4$ transition was previously observed in [30], where its amplitude was found to be roughly 1–2 orders of magnitude smaller than that of the $5 \rightarrow 4$ line. These observations indicate that the statistical uncertainty of our measurement is likely much larger than any possible contribution from other transitions, supporting the conclusion that R is a good approximation for Y and that the measured lower limit is reliable.

This lower limit is compatible with the theoretical estimate of ≈ 0.006 eV, obtained by theoretical calculation based on [11, 37].

The present work also provides a quantitative constraint that will allow future cascade calculations to be tested against data through new precise measurement of kaonic copper and fluorine transition not affected by strong interaction.

5. Conclusions

The present work reports new measurements of absolute x-ray yields for various transitions in kaonic copper and fluorine. For kaonic copper, the two most precise measurements to date are obtained for the $8 \rightarrow 7$ and $6 \rightarrow 5$ transitions, while for kaonic fluorine the absolute yields of the $5 \rightarrow 4$ and $4 \rightarrow 3$ transitions are reported for the first time. These results provide key observables that are sensitive to the atomic cascade dynamics and to the nuclear absorption.

In particular, a reduction of the yield between consecutive transitions is observed in kaonic fluorine suggesting the onset of nuclear capture at the $n = 4$ level, that led to the evaluation of a lower limit for the strong interaction in this level.

From this perspective, the present measurements complement traditional spectroscopic observables such as level shifts and widths induced by the strong interaction. With a reliable cascade model, a quantitative determination of the nuclear capture rate at these levels becomes possible, probing a regime inaccessible to shift and width measurements alone.

The measured yields also provide valuable inputs for cascade model development, in particular for constraining the role of electron refilling and the density of states during the de-excitation process, with implications across a broad range of exotic atom studies.

Finally, the present results establish CZT-based detection systems as a mature technology for high-precision kaonic atom spectroscopy, providing the experimental precision needed for yield extraction at the levels required by cascade models. This work opens a new experimental window onto the interplay of atomic cascade dynamics and nuclear absorption in kaonic atoms, establishing absolute yield measurements as a crucial experimental probe of the K–N interaction at low energies.

Acknowledgements

The authors gratefully acknowledge Riccardo Gargana for access to computational resources. We thank Jaroslava Obertova for estimating the strong interaction shifts and widths. We thank C. Capoccia from INFN-LNF for his fundamental contribution in designing and building the SIDDHARTA-2 setup. We thank as well the INFN, INFN-LNF and the DAΦNE staff in particular to Dr. Catia Milardi for the excellent working conditions and permanent support.

Data availability statement

The data that support the findings of this study are available from the corresponding author upon reasonable request. All data that support the findings of this study are included within the article (and any supplementary files).

Funding

Part of this work was supported by the Austrian Science Fund (FWF): [P24756-N20 and P33037-N]; the Croatian Science Foundation under the project HRZZ-IP-2022-10-3878; the EU STRONG-2020 project (Grant Agreement No. 824 093); the EU Horizon 2020 project under the MSCA (Grant Agreement 754 496); the Japan Society for the Promotion of Science JSPS KAKENHI Grant No. JP18H05402; the SciMat and qLife Priority Research Areas budget under the program Excellence Initiative—Research University at the Jagiellonian University, and the Polish National Agency for Academic Exchange (Grant No. PPN/BIT/2021/1/00 037); the EU Horizon 2020 research and innovation programme under project OPSVIO (Grant Agreement No. 10 103 8099). This work was also supported by the Italian Ministry for University and Research (MUR), under PRIN 2022 PNRR project CUP: B53D23024100001. This article/publication is based upon work from COST Action CA24131-ENRICH, supported by COST (European Cooperation in Science and Technology, www.cost.eu/).

Author contributions

Conceptualization, Alessandro Scordo, Carlo Guaraldo; Methodology, Francesco Artibani and Alessandro Scordo; Software, Francesco Artibani Leonardo Abbene, Antonino Buttacavoli, Fabio Principato and Alessandro Scordo; Formal analysis, Francesco Artibani; Resources, Leonardo Abbene, Manuele Bettelli, Antonino Buttacavoli, Fabio Principato, Andrea Zappettini, Johann Zmeskal and Catalina Curceanu; Data curation: Francesco Artibani, Leonardo Abbene, Antonino Buttacavoli and Alessandro Scordo; Writing—original draft, Francesco Artibani; Writing—review & editing, Leonardo Abbene, Manuele Bettelli, Antonino Buttacavoli, Fabio Principato, Andrea Zappettini, Massimiliano Bazzi, Giacomo Borghi, Damir Bosnar, Mario Bragadireanu, Marco Carminati, Alberto Clozza, Francesco Clozza, Luca De Paolis, Raffaele Del Grande, Carlo Fiorini, Ivica Friscic, Mihail Iliescu, Masahiko Iwasaki, Aleksander Khreptak, Simone Manti, Johann Marton, Paweł Moskal, Fabrizio Napolitano, Hiroaky Ohnishi, Kristian Piscicchia, Francesco Sgaramella, Michał Silarski, Magdalena Skurzok, Diana Laura Sirghi, Florin Sirghi, Antonio Spallone, Kairo Toho, Oton Vazquez Doce, Catalina Curceanu and Alessandro Scordo; Supervision, Catalina Curceanu and Alessandro Scordo; Project administration, Catalina Curceanu and Alessandro Scordo 12.

Appendix. Supplementary data

A.1. Systematics evaluation

Based on [28], the systematic uncertainties for the fit in section 3 were evaluated as follows:

1. Four additional fits were performed by shifting the calibration gain and offset by 0.0015 and 0.075, respectively. According to calibration studies reported in [21], these values correspond to the expected variations over several tens of days. The systematic uncertainty from this effect was estimated by taking the quadratic sum of the deviations from the nominal values after applying the gain and offset shifts.
2. Two additional fits were carried out by varying the energy window limits by ± 5 keV (upper limit) and ± 1 keV (lower limit), and the resulting differences were used to estimate the related systematic contribution.
3. The binning was varied by ± 5 channels, and the corresponding variation in the fitted results was recorded.
4. Finally, the total systematic uncertainty was obtained by adding in quadrature the contributions from all the independent sources listed above.

In table 6 we present the systematics for each measured quantity in the text.

Table 6. Measured values and systematic uncertainties breakdown. The systematic uncertainties are evaluated by repeating the fitting procedure under different conditions, including variations of the calibration limits and binning choices as explained in [28]. The percentage of each systematic source value to the total measured value is reported in parentheses.

Transition	Measured Quantity	Value	Stat.	Syst. (window)	Syst. (binning)	Syst. (calib.)	Syst. (total)
KF 5 → 4	Mean	23.34	0.34 (1.46%)	0.06 (0.26%)	0.02 (0.09%)	0.10 (0.43%)	0.11 (0.47%)
	Events	488	72 (14.8%)	18 (3.7%)	20 (4.1%)	13 (2.7%)	30 (6.1%)
KF 4 → 3	Mean	50.14	0.54 (1.08%)	0.19 (0.38%)	0.14 (0.28%)	0.09 (0.18%)	0.25 (0.50%)
	Events	427	74 (17.3%)	23 (5.4%)	30 (7.0%)	18 (4.2%)	42 (9.8%)
KCu 8 → 7	Mean	52.89	0.50 (0.95%)	0.22 (0.42%)	0.18 (0.34%)	0.09 (0.17%)	0.30 (0.57%)
	Events	578	84 (14.5%)	30 (5.2%)	21 (3.6%)	12 (2.1%)	38 (6.6%)
KCu 7 → 6	Mean	80.89	0.98 (1.21%)	0.39 (0.48%)	0.41 (0.51%)	0.20 (0.25%)	0.60 (0.74%)
	Events	1078	297 (27.6%)	140 (13.0%)	101 (9.4%)	80 (7.4%)	190 (17.6%)
KCu 6 → 5	Mean	134.48	0.35 (0.26%)	0.27 (0.20%)	0.12 (0.09%)	0.11 (0.08%)	0.31 (0.23%)
	Events	1206	132 (10.9%)	32 (2.7%)	25 (2.1%)	10 (0.8%)	42 (3.5%)

ORCID iDs

Francesco Artibani 0009-0000-8905-3165
Fabio Principato 0000-0003-2787-0877
Andrea Zappettini 0000-0002-6916-2716
Damir Bosnar 0000-0003-4784-393X
Francesco Clozza 0009-0002-3298-0624
Ivica Friscic 0000-0002-4743-0572
Aleksander Khreptak 0000-0002-9482-9770
Pawel Moskal 0000-0002-4229-3548
Fabrizio Napolitano 0000-0002-8686-5923
Francesco Sgaramella 0000-0002-0011-8864
Alessandro Scordo 0000-0002-7703-7050

References

[1] Friedman E, Gal A and Batty C J 1994 Density dependent K- nuclear optical potentials from kaonic atoms *Nucl. Phys. A* **579** 518–38
[2] Batty C J, Friedman E and Gal A 1997 Strong interaction physics from hadronic atoms *Phys. Rept.* **287** 385–445
[3] Cieplý A, Mai M, Meißner U-G and Smejkal J 2016 On the pole content of coupled channels chiral approaches used for the $\bar{K}N$ system *Nucl. Phys. A* **954** 17–40
[4] Curceanu C *et al* 2019 The modern era of light kaonic atom experiments *Rev. Mod. Phys.* **91** 025006
[5] Artibani F *et al* 2024 The odyssey of kaonic atoms studies at the DAΦNE collider: from DEAR to SIDDHARTA-2 *Acta Phys. Polon. B* **55** 5–A2
[6] Zmeskal J 2008 From kaonic atoms to kaonic nuclei: a search for antikaon-mediated bound nuclear systems *Prog. Part. Nucl. Phys.* **61** 512–50
[7] Aramaki T *et al* 2013 A measurement of atomic x-ray yields in exotic atoms and implications for an antideuteron-based dark matter search *Astropart. Phys.* **49** 52–62
[8] Ericson T E O and Scheck F 1970 K- nuclear interactions and yields of kaonic x-rays *Nucl. Phys. B* **19** 450–76
[9] Curceanu C, Sgaramella F, Bazzi M, Hashimoto T, Iliescu M, Scordo A, Sirghi D and Sirghi F 2026 Light kaonic atoms as probes of fundamental interactions in strange systems *Prog. Part. Nucl. Phys.* **147** 104226
[10] Friedman E and Okada S 2013 Feasibility guidelines for kaonic-atom experiments with ultra-high-resolution x-ray spectrometry *Nucl. Phys. A* **915** 170–8
[11] Óbertovà J, Ramos À and Mareš J 2025 Antikaon absorption in the nuclear medium: the role of hadron self-energies and implications for kaonic atoms *Phys. Rev. C* **112** 055201
[12] Markushin V E and Jensen T S 2001 Atomic cascade and x-ray yields in light exotic atoms *Nucl. Phys. A* **691** 318–21
[13] Koike T 2007 Cascade calculation of kaonic nitrogen atoms involving the electron refilling process *3rd Asia Pacific Conf. on Few-Body Problems in Physics (APFB05)* pp 171–4
[14] Ishiwatari T *et al* 2004 Kaonic nitrogen x-ray transition yields in a gaseous target *Phys. Lett. B* **593** 48–54
[15] Bazzi M *et al* 2013 x-ray transition yields of low-Z kaonic atoms produced in kapton *Nucl. Phys. A* **916** 30–47
[16] Bazzi M *et al* 2016 *K*-series x-ray yield measurement of kaonic hydrogen atoms in a gaseous target *Nucl. Phys. A* **954** 7–16
[17] Sgaramella F *et al* 2024 Kaonic helium-4 *l*-series yield measurement at 2.25 g/l density by SIDDHARTA-2 at DAΦNE *Acta Phys. Polon. Supp.* **17** 1–A8
[18] Sgaramella F *et al* 2025 High precision x-ray spectroscopy of kaonic neon *Phys. Lett. B* **865** 139492
[19] Abbene L *et al* 2023 Potentialities of CdZnTe quasi-hemispherical detectors for hard x-ray spectroscopy of kaonic atoms at the DAΦNE collider *Sensors* **23** 7328
[20] Abbene L *et al* 2023 New opportunities for kaonic atoms measurements from CdZnTe detectors *Eur. Phys. J. ST* **232** 1487–92
[21] Abbene L *et al* 2024 First stability characterization for a CZT detection system in an e^+e^- Collider Environment *Sensors* **24** 7562
[22] Milardi C *et al* 2009 Present status of the DAFNE upgrade and perspectives *Int. J. Mod. Phys. A* **24** 360–8
[23] Milardi C *et al* 2018 Preparation activity for the SIDDHARTA-2 *Run at DAΦNE 9th Int. Particle Accelerator Conf., IPAC2018*

[24] Milardi C *et al* 2021 DAΦNE commissioning for SIDDHARTA-2 Experiment *JACoW* **IPAC2021** TUAB001
[25] Milardi C *et al* 2024 DAFNE operation strategy for the observation of the kaonic deuterium *JACoW* **IPAC2024** WER17
[26] Sirghi F *et al* 2024 SIDDHARTA-2 apparatus for kaonic atoms research on the DAΦNE collider *JINST* **19** 11006
[27] Skurzok M *et al* 2020 Characterization of the SIDDHARTA-2 luminosity monitor *JINST* **15** 10010
[28] Artibani F and *et. al* 2026 Time-based selection of kaonic atom x-ray events with quasi-hemispherical CZT detectors at the daϕne collider *Meas. Sci. Technol.* **37** 035108
[29] Santos J P, Parente F, Boucard S, Indelicato P and Desclaux J P 2005 x-ray energies of circular transitions and electron screening in kaonic atoms *Phys. Rev. A* **71** 032501
[30] Clozza F *et al* 2026 Bound-state QED test above the Schwinger limit with kaonic fluorine (available at: http://arxiv.org/abs/2604.19387)
[31] Navas S *et al* 2024 Review of particle physics *Phys. Rev. D* **110** 030001
[32] Wiegand C E 1969 Measurement of k-minus-mesonic x-ray spectra of medium and heavy elements *Phys. Rev. Lett.* **22** 1235–8
[33] Wiegand C E and Godfrey G L 1974 MEASUREMENTS OF x-rays AND gamma RAYS FROM STOPPED KAONS *Phys. Rev. A* **9** 2282
[34] Sgaramella F *et al* 2024 First measurement of kaonic helium-4 M-series transitions *J. Phys. G: Nucl. Part. Phys.* **51** 055103
[35] Burbidge G R and de Borde A H 1953 The mesonic auger effect *Phys. Rev.* **89** 189–93
[36] Manti S *et al* 2026 Precision test of bound-state QED at intermediate Z with kaonic neon *Phys. Rev. A* **113** 022815
[37] Óbertovà J, Friedman E, Mareš J and Ramos A 2022 On K^--nuclear interaction, K^--nuclear quasibound states and K^- atoms *EPJ Web Conf.* **271** 07003